Friction between Polymer Brushes in Good Solvent Conditions: Steady-State Sliding versus Transient Behavior

Torsten Kreer and Kurt Binder

Institut für Physik, WA 331, Universität Mainz, 55099 Mainz, Germany

Martin H. Müser*

Department of Applied Mathematics, University of Western Ontario, London, Ontario N6A 5B7, Canada

Received January 10, 2003. In Final Form: May 27, 2003

Previous molecular dynamics simulations of friction between polymer brushes in relative sliding motion [Kreer, T.; Müser, M. H.; Binder, K.; Klein, J. *Langmuir* **2001**, *17*, 7804] are extended beyond steady-state conditions. We study two different protocols: (i) stop and return and (ii) stop and go. In protocol (i), the relative, lateral motion between the two surfaces is stopped abruptly and reimposed opposite to the initial direction after the system could relax for some time. Protocol (ii) is similar except that the sliding direction is maintained. In the constant-velocity steady state, the average lateral extension l_c of the polymers is found to be a power law of the sliding velocity v, namely, $l_c \propto v^{0.3}$. When the sliding direction is inverted, a shear stress maximum is observed after the two walls have slid a relative distance of $2l_c$. This maximum occurs when the average inclination of the polymers is 90°, and it is accompanied by brush swelling. In protocol (ii), no brush swelling is found and shear stress maxima are absent in the itinerant stages of the go phase, with the exception of large v. We conclude that dissipation mechanisms for oscillatory shear are similar to those for constant-velocity sliding if the driving amplitude $\mathcal{A}$ distinctly exceeds $2l_c$. Moreover, enhanced loss at $\mathcal{A} \approx 2l_c$ is not necessarily related to stick−slip motion.

I. Introduction

The present study, which is an extension of previous molecular dynamics simulations,[1] is motivated by the desire to better understand friction between two solid surfaces bearing polymer brushes in good solvent conditions. Revealing the atomistic origins of friction and lubrication in such systems is an active field of research both experimentally and in terms of computer simulations; for reviews, see for instance refs 2 and 3. The pioneering experiments by Klein et al.[4,5] of surfaces bearing polymer brushes showed strikingly small effective, kinetic friction coefficients μ (as defined by the traditional equation μ equals friction force divided by load) in the steady-sliding regime. Computer simulations by Grest confirmed the intuitive picture that sliding-induced chain "stretching and disentanglement" of the polymers is responsible for the small values of μ.[6] Since chains that are as short as those commonly used in computer simulations cannot entangle,[7] it might be more appropriate to relate this extreme shear thinning to "stretching and inclination" and a concurrent decrease in the mutual overlap between the polymer brushes.[1]

The above-mentioned studies on friction between brushes address stationary sliding, and a clear, qualitative picture has emerged for steady-state friction between brushes in good solvent conditions. However, oscillatory driving and the crossover behavior between two different sliding states are certainly also important to study, in particular as little is known about the atomistic processes occurring under oscillatory shear or during nonstationary driving. To the best of our knowledge, most numerical studies focus on normal forces rather than lateral forces. For example, Doyle et al.[8] investigated brush swelling in order to explain the experimentally observed increase in the normal forces;[5] however, no detailed, atomistic analysis of the interplay between rheology (interdigitation, inclination, end-to-end distance, etc.) and shear forces is known to us for our system of interest.

Experimental studies by Granick, Cai, and co-workers[9,10] employing oscillatory shear between brushes under near theta-solvent conditions suggested that there are regimes of enhanced dissipation for certain driving amplitudes at fixed frequency or, alternatively, enhanced dissipation for certain frequencies at fixed amplitudes. In linear response, such enhanced dissipation can be related to an (approximate) coincidence of relaxation times and inverse driving frequencies.[11] Zaloj et al. suggested an

* To whom correspondence should be addressed. E-mail: mmuser@uwo.ca.

(1) Kreer, T.; Müser, M. H.; Binder, K.; Klein, J. *Langmuir* **2001**, *17*, 7804.
(2) Klein, J. *Annu. Rev. Mater. Sci.* **1996**, *26*, 581.
(3) Grest, G. S. In *Polymers in Confined Environments*; Granick, S., Ed.; Advances in Polymer Science 138; Springer: Berlin, 1999; p 149. Grest, G. S.; Murat, M. In *Monte Carlo and Molecular Dynamics Simulations in Polymer Science*; Binder, K., Ed.; Oxford University Press: New York, 1995; p 476.
(4) Klein, J.; Kumacheva, E.; Mahalu, D.; Perahia, D.; Fellers, L. J. *Nature* **1994**, *370*, 634.
(5) Klein, J.; Parahia, D.; Warburg, S. *Nature* **1991**, *352*, 143.
(6) Grest, G. S. *Phys. Rev. Lett.* **1996**, *76*, 4979.
(7) Kreer, T.; Baschnagel, J.; Müller, M.; Binder, K. *Macromolecules* **2001**, *34*, 1105.
(8) Doyle, P. S.; Shafeh, E. S. G.; Gast, A. P. *Macromolecules* **1998**, *31*, 5474. Doyle, P. S.; Shafeh, E. S. G.; Gast, A. P. *Phys. Rev. Lett.* **1997**, *78*, 1182.
(9) Granick, S.; Demirel, A. L.; Cai, L. L.; Peanasky, J. *Isr. J. Chem.* **1995**, *35*, 75.
(10) Cai, L. L.; Peanasky, J.; Granick, S. *Trends Polym. Sci.* **1996**, *4*, 47.
(11) Luengo, G.; Schnmidt, F.-J.; Hill, R.; Israelachvili, J. *Macromolecules* **1997**, *30*, 2482.

10.1021/la030008x CCC: $25.00
Published on Web 07/26/2003

alternative mechanism for the occurrence of enhanced dissipation.[12] Taking into consideration the elastic coupling of the driving device to an embedded (frictional) system, they showed that stick−slip motion can occur at intermediate driving amplitudes $\mathcal{A}$, which would then explain the observed enhanced dissipation. Both at small $\mathcal{A}$ and at large $\mathcal{A}$, friction would be smaller, because the embedded particle's motion is smooth in either limit. Zaloj et al. supported their claim by studying a simple linear molecule, embedded between two shearing plates. While Zaloj et al.'s scenario for enhanced dissipation is certainly legitimate, it is not necessarily the relevant mechanism for our system of interest and a more accurate model is needed to clarify the mechanism.

Another important study on itinerant effects in good solvent conditions was reported by Tadmor et al.[13] They studied the effect of waiting time on the itinerant friction, once sliding was reinitiated in the direction opposite to the initial sliding direction. They found an increase in friction with waiting time and argued that this increase is due to the mutual interpenetration of the brushes, which increased with increasing waiting time.

In this paper, we intend to contrast rheological and tribological properties for stationary and nonstationary sliding of polymer brushes in good solvent conditions. As in our preceding paper, special emphasis is placed on the interplay between shear forces σ_{br} and the mutual brush interdigitation. Nonstationary sliding is realized in two different manners, namely, protocol (i), "stop and return", and protocol (ii), "stop and go". In both modes, we start from steady-state sliding at velocity v and bring the relative, lateral motion of the two confining walls to an immediate stop. The system can then relax for some time t_{rel}. In most cases, we chose t_{rel} larger than the time that σ_{br} needs to decay to zero within statistical uncertainty. Sliding is then reinitiated with the same absolute velocity as before, which is (i) opposite to or (ii) along the old sliding direction. Such a protocol will allow us to perform a detailed investigation of the transient behavior that occurs after relaxation and/or after inversion of v.

One of the goals in this study is to analyze the effect of nonstationary sliding on the interdigitation I of the brushes and the concurrent induced changes in the shear stresses σ_{br}. In ref 1 (Figure 9), we observed a surprisingly large correlation between I and σ_{br}: the effect on σ_{br} due to large momentum transfers between monomers at large sliding velocities was almost exactly balanced by the inclination of the polymers. As a result, σ_{br} was nearly a unique function of I within a large parameter space, in which many parameters were varied significantly such as grafting density, solvent viscosity, and sliding velocity. The interplay between interdigitation and shear forces during nonstationary sliding will therefore also be central to this study.

The remainder of this paper is organized as follows: In the following section, the simulation method, the features of the model, and the most important observables are discussed. Section III contains the results of our simulations. We will first provide information on steady-state sliding that is complementary to our previous work. Then, the analysis of shear stress relaxation will be presented as well as rheological and tribological behavior when sliding is reinitiated. Section IV contains the conclusions.

(12) Zaloj, V.; Urbakh, M.; Klafter, J. *Phys. Rev. Lett.* **1998**, *81*, 1227.
(13) Tadmor, R.; Janik, J.; Fetters, L. J.; Klein, J. Private communication, 2002.

II. Method, Model, and Observables

In this study, we perform standard molecular dynamics (MD) simulations of a coarse-grained model, which is well established for the investigation of friction between polymer-bearing surfaces.[3] The polymers consist of bead−spring chains, where appropriate potentials ensure excluded volume interactions between the beads as well as the connectivity along the backbone of the chain. These potentials are the Lennard-Jones potential

$$U(r) = 4\epsilon\left[\left(\frac{\sigma}{r}\right)^{12} - \left(\frac{\sigma}{r_c}\right)^{12} - \left(\frac{\sigma}{r}\right)^{6} + \left(\frac{\sigma}{r_c}\right)^{6}\right] \qquad (1)$$

where r_c is the interaction cutoff radius, and the finitely extensible nonlinear elastic (FENE) potential

$$U_{FENE}(r) = \begin{cases} -0.5kR_0^2 \ln[1 - (r/R_0)^2] & r \le R_0 \\ \infty & r > R_0 \end{cases} \qquad (2)$$

where $R_0 = 1.5\sigma$, $k = 15\epsilon/\sigma^2$, and r is the distance between adjacent particles. ϵ and σ are characteristic energy and length scales, respectively. One end of each polymer is tethered to a random position on one of the two atomically smooth surfaces. Both surfaces bear the same amount of grafted polymers. The solvent is not treated explicitly, but in terms of a Langevin thermostat. Including solvent atoms would slow the simulations distinctly and prevent us from accessing the relevant length and time scales. As done previously, good solvent conditions are mimicked by the effective interactions between monomers. By choosing a cutoff radius of $r_c = 2^{1/6}\sigma$, we allow only for repulsive interactions. This choice is often referred to as the athermal case. All data presented in the following figures are expressed within the Lennard-Jones units of ref 1. Note that in order to compare our results with experiments, it will be necessary to scale length and time scales in a meaningful way, because the polymers used in experiments have a much larger degree of polymerization N than in our simulations. This issue is also discussed in more detail in ref 1.

There is one important modification of our simulations with respect to ref 1. In our previous study, the thermostat acted within the laboratory system. This created a small asymmetry in the structures of the two opposing brushes, because the upper brush was moved and hence dragged through the solvent, while the lower brush remained fixed in the laboratory system. In the new series of simulations, we switch off the thermostat parallel to the shear direction, because we do not want to bias or to impose any (effective) solvent flow in the sliding direction. This change has two additional motivations: First, in our previous work we overestimated the effect of solvent flow into the brushes, while in this work we underestimate the flow. If both methods yield similar results for the rheology and the tribology of the brushes, one may be confident that there are no relevant, systematic artifacts. Second, during the stop phase of our simulations, we want to analyze the relaxation of the brushes. With our previous choice of the thermostat, the signal-to-noise ratio is less good and, in addition, relaxation times are larger than with our new choice of thermostating only normal to sliding. As it turns out, however, the qualitative effects of the above-mentioned alteration on the shear forces between the brushes are rather minor; merely quantitative details are affected. This could be expected, because our system is highly viscous and thus far from a fluid at large Reynolds numbers, for which this issue would be critical. To avoid underestimating heat transport, we leave the thermostat

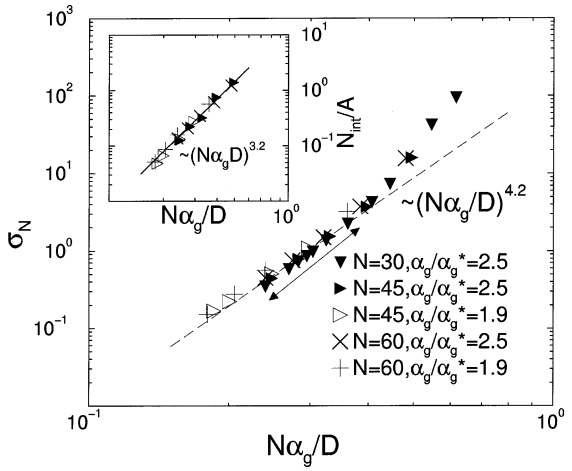

Figure 1. Normal stress σ_N as a function of an effective density $N\alpha_g/D$ between the two confining walls for different degrees of polymerization N and grafting densities α_g. The arrow encompasses the regime of the shear simulations presented below. The dashed line reflects a power law $D^{-4.2}$. Inset: Surface density of the number of interactions per area N_{int}/A as a function of the scaled inverse separation. N_{int} counts the number of interactions between monomers belonging to the upper brush and monomers attributed to the lower brush.

switched on in the directions normal to sliding. A more detailed discussion is given in section III.A.

The grafting densities α_g employed in this study range between 1.9 α_g^* and 2.5 α_g^*, where $\alpha_g^* = 1/\pi R_{gyr}^2$ denotes the critical grafting density and R_{gyr} is the radius of gyration of a single free chain in solution. At α_g^*, chains are starting to overlap which leads to stretching of the polymers perpendicular to the walls. The simulations of this study are carried out in a regime of large compression. The dependence of the normal stress σ_N on the distance D between the surfaces can be approximated rather well by a power law $\sigma_N \propto (N\alpha_g/D)^{4.2}$, which is shown in Figure 1. This empirical exponent agrees rather well with the situation encountered experimentally, although here the brushes are only compressed by about a factor of 2−3 with respect to the unperturbed brush. This is much less than typical experimental compressions, but owing to the relatively small degree of polymerization in the simulations, we obtain the correct scaling at smaller absolute values of the compressions than in experiment.

Most of our simulations are done in the regime marked by the arrow in Figure 1, where $30 \le N \le 60$, $1.9 \le \alpha_g/\alpha_g^* \le 2.5$, and $D = 17.5$, unless mentioned otherwise. Despite the relatively strong increase of σ_N with increasing effective density $N\alpha_g/D$, it is not yet possible to define static friction in a meaningful way. The reason is that the lateral motion between the walls behaves as diffusive or subdiffusive when no external shear force is applied to the system.

Using the units of ref 1, the smallest shear velocity $v = 0.01$ used in this study corresponds roughly to $v \approx 1$ m/s. It is necessary to keep in mind that the comparison of absolute velocities between simulations and experiments is often rather meaningless within a tribological context. Instead it is more meaningful to compare results in which the ratios of characteristic distance and characteristic time are similar.[14] Characteristic times increase with N rather rapidly, and as a consequence our results shall be compared to experimental sliding velocities much smaller than 1 m/s, because experimental values for N are usually distinctly larger than those used in the simulations (namely, $N = 30-60$ effective segments).

Figure 1 also includes information on the mutual interdigitation of brushes in thermal equilibrium, which turned out to be a central quantity in our preceding work. We specify the amount of interdigitation using two different observables, namely, the number of interactions N_{int} and the overlap integral I. N_{int} is counted by adding up the number of pairs of monomers where the two monomers belong to different brushes and where the distance between the monomers is smaller than a characteristic, atomic-scale distance r_c. We chose r_c to be identical with the cutoff radius of the potential, which is slightly larger than the separation between two adjacent monomers on the polymer backbone. N_{int} can be written as

$$N_{int} = \sum_{\substack{i \in \text{lower brush} \\ j \in \text{upper brush}}} \Theta(r_{ij} - r_c) \qquad (3)$$

where r_{ij} denotes the separation between monomer i and monomer j, and Θ is a step function, which is 1 if its argument is negative and 0 for a positive argument. The definition of N_{int} differs slightly from the one given before in eq 10 of ref 1. The overlap integral I is defined as the integral of the product $\rho_{ub}(z)\rho_{lb}(z)$ over z, where z denotes the coordinate normal to the interface and $\rho_{ub}(z)$ and $\rho_{lb}(z)$ denote the monomer density of the upper and lower brush, respectively. To a good approximation, N_{int} is proportional to I. For our data related to $D = 17.5$ and $\alpha_g/\alpha_g^* = 2.5$, we find $N_{int}/A \approx 825I$. Including an offset and a term quadratic in I improves the fit by less than 5%.

The other central quantity of this study is the shear stress σ_{br} between the brushes. This observable is evaluated directly at the interface of the two grafted layers, thus

$$\sigma_{br} = \frac{1}{A} \sum_{\substack{i \in \text{lower brush} \\ j \in \text{upper brush}}} F_{||}(r_{ij}) \qquad (4)$$

where A is the area of contact and $F_{||}(r_{ij})$ is the force between monomers parallel to the sliding direction. Equation 4 allows us to calculate *non*stationary shear stresses with much higher sensitivity as if σ was evaluated at the confining walls, because the signal is smeared out less. In the case where one calculates the friction at the wall, one has to sum up the forces between the particles constituting the embedded system and those constituting either the upper wall or the lower wall. This means that in eq 4 the index i would run over all monomers and index j would run over all wall atoms. In steady-state sliding, the resolution of σ does not depend on the way in which σ is determined. As just mentioned, evaluating shear at the wall leads to a signal which is smeared out more than if the shear is evaluated directly between the two brushes. Due to the much smaller sliding velocities in experiments, the smear-out effect must be smaller than in our simulations, where run-time effects play a more significant role than in typical experimental situations.

III. Results

A. Steady-State Sliding, Revisited. One important modification of our simulations with respect to our previous investigation[1] of shear stresses between polymer-bearing surfaces at constant velocity concerns the thermostat. Here, it no longer acts parallel to the sliding direction, which we always chose parallel to the x-axis. As

(14) Müser, M. H. *Comput. Phys. Commun.* **2002**, *147*, 83.

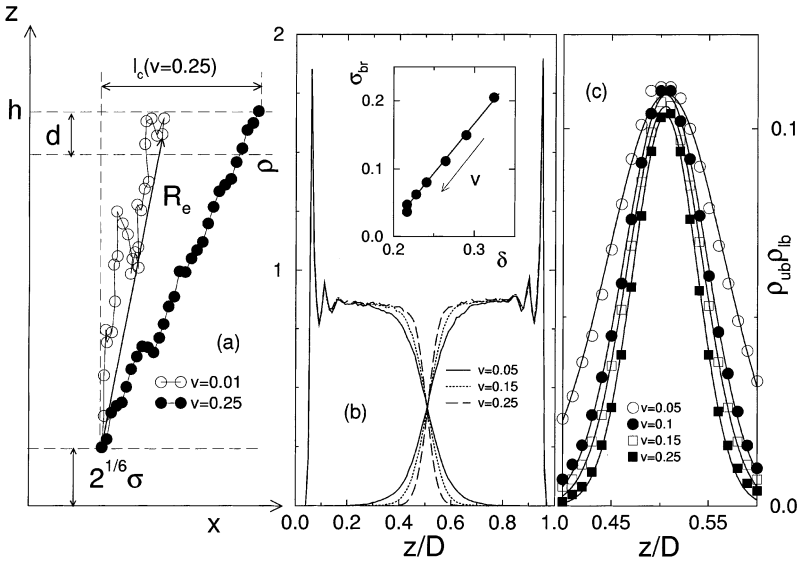

Figure 2. (a) Configuration of randomly chosen polymers at two different sliding velocities projected onto the (*xz*) plane. (b) Density profile of upper and lower brush. Inset: Shear stress σ_{br} between brushes as a function of overlap distance δ. (c) Folded density profile. The lines are fits to the data according to $\rho_{lb}\rho_{ub} \propto \exp[-(z/D - 0.5)^2/\delta^2]$, which defines δ.

discussed in the Introduction, this means that we now underestimate the solvent flow into the brushes while we overestimated it in our preceding study. We will show here that this change does not have qualitative implications for the shear forces between the brushes and that the rheology of the brushes is altered only slightly. More importantly, we will also alter the degree of polymerization and grafting density to see how these parameters affect the shear forces between the brushes.

The shear alignment of the polymers, as shown by a snapshot in Figure 2a, is now entirely induced by the brush−brush interaction, while it was also induced through the solvent flow before. Increasing the sliding velocity reduces the mutual brush interpenetration. This can be seen in Figure 2b, which contains the density profiles of the individual brushes for different sliding velocities. The folded density profiles $\rho_{lb}(z)\rho_{ub}(z)$ now can be approximated rather well by a Gaussian $\exp[-(z/D - 0.5)^2/\delta^2]$ as demonstrated in Figure 2c.

Due to the altered thermostat, the folded density profiles are now much more symmetric than previously; see Figure 7 in ref 1. Another difference concerns the folded density profile in the middle of the interface $z = D/2$, which decreases considerably less with increasing shear velocity than in our previous treatment. Despite these discrepancies, important results remain unaltered. In particular, the shear stress between the brushes decreases with increasing shear velocity, as shown in the inset of Figure 2b. Also, the large correlation between overlap and shear force persists in our new treatment, which is demonstrated in more detail in Figure 3, where we also varied the degree of polymerization N as compared to our previous study. The coupling of the brushes to the solvent is treated like in our previous approach within one data set of Figure 3, but the corresponding data fall on the same curve as the new data. Only changing the grafting density (in units of the critical grafting density α_g^*) apparently causes a significant deviation from the original curve.

The data shown in Figure 3 exhibit an almost logarithmic velocity or shear-rate dependence of N_{int} within the limited range of velocities accessible to the simulations, as shown in Figure 4. This is consistent with the logarithmic shear-rate dependence of the shear force, which is discussed in more detail in a separate study by some of the present authors,[15] which focuses especially on relaxation processes after the sliding motion is stopped abruptly. Note that the shear forces presented here do not include the coupling of the brushes to the solvent flow, as the solvent is not treated explicitly in our study. Thus,

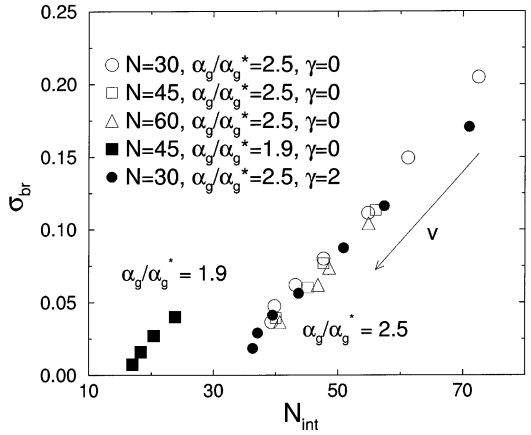

Figure 3. Shear stress σ_{br} as a function of brush interdigitation as measured by the number of interactions N_{int}. Data from previous work, in which the thermostat also acted along the sliding direction ($\gamma = 2$), are included in the figure.

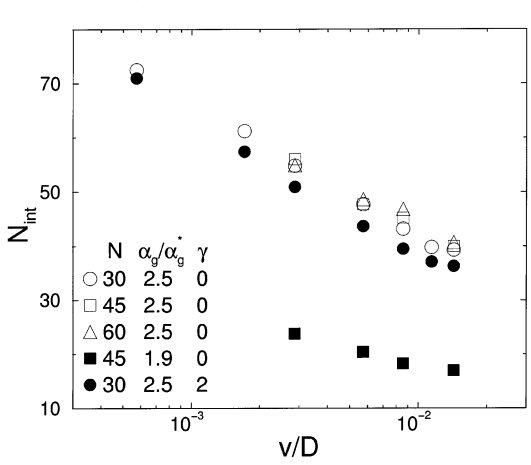

Figure 4. Number of interactions between opposing brushes as a function of shear rate.

the experimental verification of the logarithmic shear-rate dependence of N_{int} and σ_{br} will be difficult if grafting densities are small and sliding velocities are large. Under such circumstances, the measured shear might be dominated by the solvent flow into the brushes.

Of course, the velocity range, in which the logarithmic behavior shown in Figure 4 can be observed, must be limited both at large and at small velocities. At sufficiently small velocities, linear response theory will apply and hence changes in N_{int} must be linear in v. We do not have an estimate for the velocities where the crossover between the linear response and the logarithmic regime takes place. At large velocities, N_{int} must remain positive, and thus the velocities where the logarithmic dependence of N_{int} on v must break down can easily be estimated from Figure 4. The discussion of both limits, $v \to 0$ and $v \to \infty$, relies neither on brush swelling/shrinking nor on constant load/separation constraints.

Figures 2−4, which focus on mutual brush interpenetration, confirm the validity of the conclusions from previous works for the new thermostat conditions. However, as noted in the Introduction, sliding-induced inclination may also be responsible for small friction between brushes. Figure 2 alludes to this effect. The inclination of the polymers can be characterized by the projection of the end-to-end vector of the polymers onto the sliding direction. This characteristic length l_c can be expected to become important when sliding is reversed, as one has to pull at least a few times this distance before steady state can be achieved again. We find that the characteristic distance shows power-law behavior as a function of sliding velocity, which will be discussed next. The regime where power-law behavior can be observed must eventually break down both at small and at large velocities. At very small velocities, linear response must be valid and a linear relation between inclination and sliding velocity follows. At very large velocities, the chains are fully stretched. In our model, a strict upper bound for the maximum covalent bond length is given through the FENE potential.

B. Stop and Return. When the sliding direction is reversed, chains will have to reorient. After the upper wall is moved a sufficiently large distance in the new direction, the chains will be in the new steady state, which is a mirror image of the original steady state. In between, polymers must pass through a configuration where the inclination is 90°, which means that the end-to-end vector is perpendicular to the walls. The time at which the expectation value of the inclination is 90° is a characteristic time, which we call τ_Φ in the following. Here, we disregard the spatial extension of the polymer in the y direction, which always turned out to be small compared to the steady-state characteristic length l_c, with maybe the exception of the smallest sliding velocities. Alternatively, one may argue in terms of ensemble averages, in which case the definition of τ_Φ can remain the same, while the first moment of y automatically disappears for symmetry reasons.

One may estimate τ_Φ from a simple geometric consideration based on Figure 2a. Imagine a configuration where the (nongrafted) endgroups of two polymers belonging to opposing walls are close to each other. The (grafted) headgroups of the polymers then have a lateral displacement of $2R_e\cos(\Phi)$ parallel to the sliding direction, which allows one to define a characteristic length $l_c = R_e\cos(\Phi)$. One has to pull the upper wall precisely by $2l_c$, to bring the two grafted headgroups of the two polymers under consideration on top of each other, which requires sliding in the reverse direction for a time $2l_c/v$. Taking into account inertia of the chain and/or damping effects, one would expect $2l_c/v$ to be an upper estimate for τ_Φ. However, considering the thermodynamic driving force, which prefers the (average) end-to-end vector to be perpendicular to the walls, one would expect $2l_c/v$ to be a lower estimate for τ_Φ. If both effects are small or cancel approximately, one obtains

$$\tau_\Phi(v) \approx 2\frac{R_e\cos\Phi}{v} \tag{5}$$

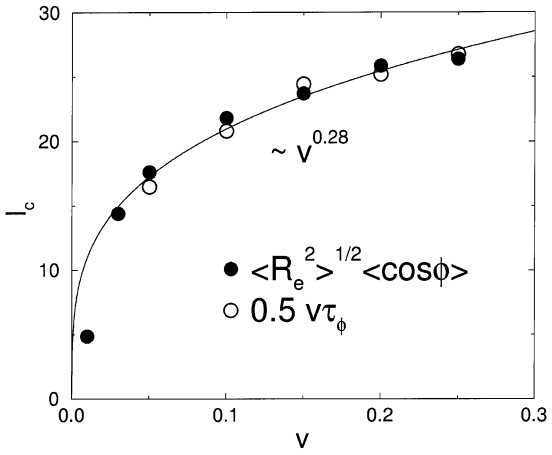

Figure 5. Characteristic length l_c as a function of velocity. Closed points denote the values taken from steady-state examinations, and open symbols refer to our direct measurements of the characteristic times during reverse sliding. The solid line reflects the power law $v^{0.28}$.

This estimate turns out to be a surprisingly good description of the correlation between τ_ϕ and l_c, as can be seen in Figure 5, where we compare the characteristic length l_c as determined in steady-state sliding with the product of characteristic time τ_ϕ and sliding velocity v of the stop-and-return protocol.

Over some range of velocities, the characteristic length obeys a power law $l_c \propto v^{0.3}$ as a function of sliding velocity, which is a reflection of the far-from-equilibrium nature of the simulations. This power-law relation can only be an approximation within a limited shear-rate window. The limits of the validity of $l_c \propto v^{0.3}$ are imposed through the linear response regime at small shear rates and through fully stretched chains at large shear rates. While the exponent 0.3 is not found to be universal, that is, it depends on N and α_g, it would be interesting to check the power experimentally. As we will show later, the shear force maxima occur almost simultaneously with the condition that the average inclination passes through 90°. Unfortunately, it is not obvious to us what determines the precise value of the exponent in the power law $l_c \propto v^{0.3}$. One of the difficulties in the derivation of this power law would be the nontrivial dependence of the overlap and hence the shear force on the relative sliding velocity.

The behavior of the polymer's inclination during the itinerant stages of the return phase can be characterized in terms of a crossover function $C_c(t)$, which we define as

$$C_c(t) = \frac{\Phi(t) - 90°}{\langle\Phi\rangle_{ss} - 90°} \tag{6}$$

where the time $t = 0$ is defined as the moment at which sliding is reversed, and $\langle\Phi\rangle_{ss}$ denotes an expectation value in the new steady state. Hence, for an abrupt change of velocity from $-v$ to v, $C_c(0) = -1$ and $C_c(t \to \infty) = 1$. As

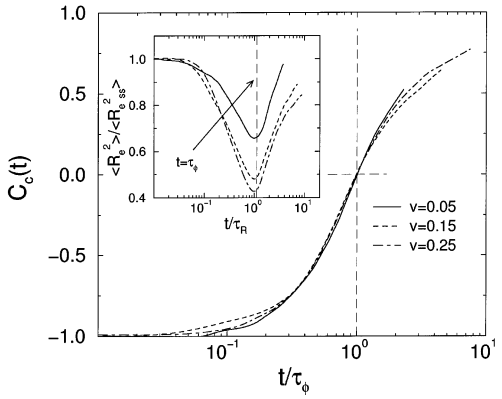

Figure 6. Crossover function $C_c(t)$ defined in eq 6 as a function of normalized time t/τ_Φ during stop-and-return for various sliding velocities. Inset: Time dependence of the end-end distance R_e normalized by the steady-state values.

shown in Figure 6, the general behavior of the crossover function is rather independent of the sliding velocity v.

It is also interesting to study the absolute value of the end-to-end vector R_e, which is shown in the inset of Figure 6. For this purpose, it is convenient to introduce a new characteristic time τ_R, which is defined as the time elapsed between the moment where the sliding direction is inverted and the moment at which the expectation value of R_e is minimal. It is obvious that the polymers are strongly compressed during the return phase. This requires energy, which will eventually be dissipated as heat. An increase of the relative (and hence absolute) compression of the polymers is observed with increasing sliding velocities. We may note in passing that τ_R and τ_Φ are strongly correlated; that is, for our data we found $\tau_R \approx 0.9\tau_\Phi$. The data for the compression in the inset of Figure 6 superimpose less systematically than for the inclination angle shown in the main part of Figure 6.

A question discussed in the literature is whether brushes swell or shrink when slid against each other. Previously, we found almost constant brush heights for constant-velocity sliding,[15] supporting the theory of Rabin and Alexander.[16] One can conclude from Figure 6 that R_e decreases upon return, while sin(Φ) goes through a maximum; hence a more detailed analysis is necessary to find the behavior of the product $R_e \sin(\Phi)$, which gives the brush height. Such an analysis is shown in the top of Figure 7, in which the solid line reflects the theory of Rabin and Alexander, who predicted constant brush heights for constant-velocity sliding. One can see that the curves clearly lie above that line, indicative of brush swelling. Our data do not include the return to steady-state, constant-velocity sliding, which would require the data to join the Rabin−Alexander line again. The observation of brush swelling during the return phase is in agreement with Doyle et al.'s simulations of oscillatory shear.[8] They suggested that swelling is due to a diffusive process of monomers into the overlap region, which is consistent with our observations concerning the return protocol.

The bottom part of Figure 7 shows snapshots of the polymers during the return phase. The snapshots are separated by time intervals $2\tau_\Phi$, and time progresses from the left to the right. It can be seen that the inclination of both polymers is approximately 90° after $2\tau_\Phi$; however, a memory or hysteresis in the structure of the polymer

(15) Kreer, T.; Müser, M. H. *Wear*, in press.
(16) Rabin, Y.; Alexander, S. *Europhys. Lett.* **1990**, *13*, 49.

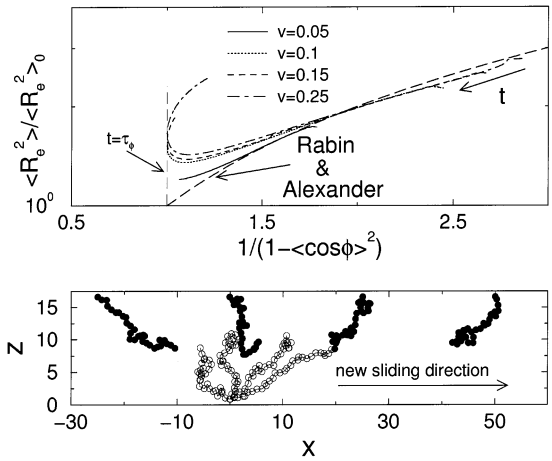

Figure 7. Top: Comparison between inclination angle and end−end distance during the transition $v \rightarrow -v$. Bottom: Time evolution of a randomly chosen chain from the upper brush (filled symbols) and the lower brush (open symbols) during crossover to a new steady state.

belonging to the upper wall persists even after the upper wall has been slid by a distance $6\tau_\Phi v$.

As the brushes swell during the return phase, the mutual brush interpenetration or the overlap should be large. Keeping in mind the correlation between brush overlap and shear forces for the steady-sliding regime, shear forces thus must be high during swelling. These conclusions are confirmed in Figure 8. In the top row, we show the overlap (as measured by N_{int}) as a function of time t without (left) and with (right) giving the system time to relax. The bottom row shows the corresponding shear forces σ_{br}. As expected, both N_{int} and σ_{br} are maximal after sliding in the new direction was imposed for a time τ_ϕ. This means that both quantities are maximal when the average inclination angle Φ is approximately 90°.

The inset of Figure 8 shows the waiting-time dependence of the maximum shear force during the itinerant phases of return. While an increased maximum shear stress is detected for the waiting time $t_{rel} = 50$, our data suggest that the overshoot decreases eventually. However, it is very difficult to get good statistics due to the poor signal-to-noise ratio. All the data presented in Figure 8 are the averages over 10 independent simulations of a system containing 3990 particles, where each single run is 10^5−10^6 MD steps long. One may yet speculate that the relatively weak dependence of the maximum in σ_{br} on the relaxation time t_{rel} might be due to the fact that the driving forces in our system are essentially entropic, while in experimental systems,[13] energy relaxation could induce the logarithmic increase of the maxima in σ_{br} with t_{rel}. Processes requiring energy activation such as cis−trans conformation changes are not included in our model.

From our results on the itinerant behavior during the return phase, it is possible to draw some semiquantitative conclusions on oscillatory shear. For this purpose, we make the thought experiment of moving the upper wall a distance $2\mathcal{A}$ at constant velocity v in one direction. We then suddenly invert the sliding direction and move again the same distance, whereupon we reiterate the procedure. This thought experiment would roughly mimic rheological driving with amplitude $\mathcal{A}$ and period $T = 4\mathcal{A}/v$ or alternatively frequency $\omega = \pi v/2\mathcal{A}$. In our thought experiment, one would expect friction to be large if the dissipated energy per area and slid distance $\{\int dx\sigma(x)\}/\int dx$ is maximal. Here, x denotes the distance that the upper wall has moved parallel to the new direction since the last return; hence $\int dx = 2\mathcal{A}$ between two returns.

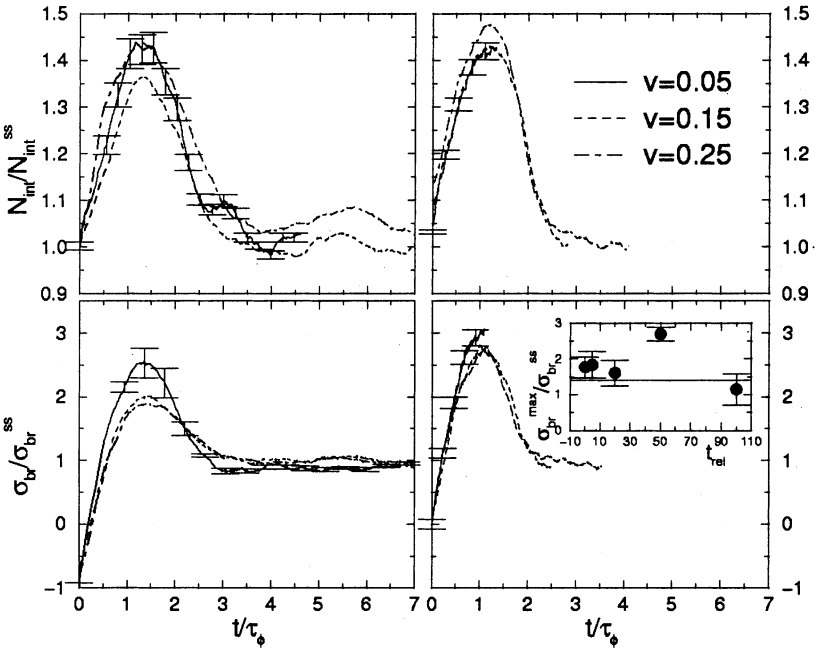

Figure 8. Number of interactions (top row) and direct shear stress between brushes (bottom row) normalized by their steady-state values for $t_{rel} = 0$ (left colon) and $t_{rel} = 50$ (right colon) during reversal sliding. Error bars are given for $v = 0.05$ and are equal or smaller for higher velocities. Inset: Height of the maximum for $v = 0.2$ as a function of waiting time. The horizontal line denotes the value for $t_{rel} = \infty$, i.e., sliding is initiated out of thermal equilibrium ($v = 0$).

From the lower part of Figure 8 (left-hand side), one would expect maximum friction if the net distance moved per semicircle ($2\mathcal{A}$) would presumably be close to but less than $2\tau_\Phi v$. This rough estimate would also follow from the bottom part of Figure 6. A similar result, maybe a slightly lower value for the "optimal" amplitude $\mathcal{A}$, would be obtained if our goal was to maximize the mutual brush overlap; see the upper part of Figure 8 (left-hand side). All these estimates anticipate that the characteristic driving amplitude $\mathcal{A}_c$ defined by

$$\mathcal{A}_c = v\tau_\Phi \propto v^{0.3} \tag{7}$$

maximizes the energy loss. For $\mathcal{A}$ much greater than $\mathcal{A}_c$, steady state would be reached. In steady state, there is less resistance to sliding than during large fractions of the itinerant return phase. For $\mathcal{A} \ll \mathcal{A}_c$, shear stresses would not even reach the steady-state value and hence energy loss would be small as well. This power law might be related to the time needed to reach steady-state conditions if one starts from equilibrated configurations at $v = 0$; see for instance the introduction in ref 17.

If we incorporate the power law $l_c \propto v^{0.3}$ (shown in Figure 5) into our conclusions, then we expect the characteristic driving amplitude $\mathcal{A}_c$, for which the dissipation is maximal, to scale with $v^{0.3}$; see eq 7. Here v is the maximum velocity in oscillatory driving. Alternatively, the frequency at which friction is maximum is expected to scale with a power law close to $v^{0.7}$, where v is again the maximum velocity during the rheological experiment. Of course, this prediction is only an approximation and it can only hold in the velocity range where the power law $l_c \propto v^{0.3}$ is a reasonable description.

We want to conclude this section with a comment on the two ensembles constant separation, which was our choice, versus constant load. While we consider constant load to be closer to many technical applications, constant separation is often imposed in experiments, in particular when normal forces are measured and hence applied to the system under investigation. Although we intend to interpret experimental results, it is still necessary to discuss the consequences of stop-and-return under constant-load conditions. When we reverse sliding, we observe an increase in the normal force between the upper and lower brushes in the order of 10%. This observation clearly demonstrates that the constant load and the constant separation ensembles are not identical. Moreover, it shows once more that it is often not possible to properly define a friction coefficient under constant separation,[14] in particular in the stop-and-return protocol, where it is even difficult to define a meaningful average load. However, the brushes are very soft, which allows them to accommodate the additional normal force rather easily. In a few test runs at constant load, we noted that the relative corrections to the shear force and other observables of interest such as the compression of the polymers were even smaller than those in the normal force. This means that there are only small quantitative changes rather than qualitative changes, when we move from constant separation to constant load; that is, the shear force overshoot would be reduced from a 100% overshoot to an overshoot in the order of but greater than 90%.

C. Stop and Go. While inversion of the driving direction leads to a strong deviation from steady-state sliding, effects are more subtle when sliding is reimposed in the original direction after some waiting time t_{rel}. Of course, in the limit of $t_{rel} \to \infty$ the protocols (i) stop, 'wait', and *return* and (ii) stop, 'wait', and *go* must lead to the same behavior. However, as relaxation times are extremely large in compressed brushes, the relaxation to the zero-stress equilibrium structure is hardly ever reached.

The relaxation after stopping for our model system has already been investigated in ref 15. The inset of Figure 1 in that paper shows that the brushes essentially relax along the Rabin−Alexander line, while inversion of the sliding direction leads to brush swelling as demonstrated in the top part of Figure 7. Here, we will be concerned with the question of how the system goes back into steady

(17) Kröger, M.; Loose, W.; Hess, S. *J. Rheol.* **1993**, *37*, 1057.

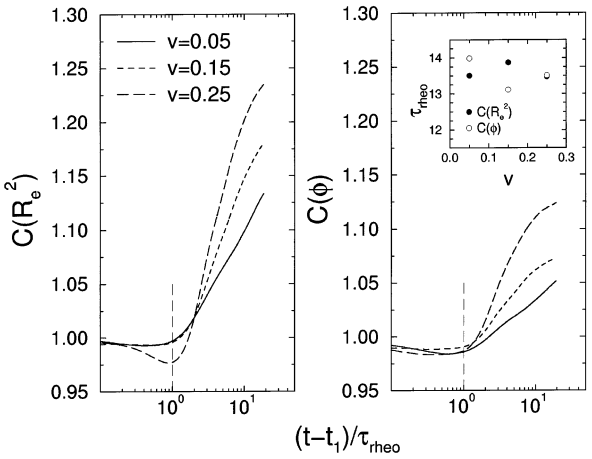

Figure 9. Transition functions of rheological observables for the stop-and-go protocol. The time axis is rescaled by the characteristic time τ_{rheo}, defined as the time where $\partial C(t)/\partial t$ becomes positive. At time $t = t_1$, sliding is reinitiated after the system could relax for a time $t_{rel} = 50$. Left: Squared end-to-end distance. Right: Inclination angle. Inset: Characteristic time as a function of velocity.

sliding after it was given the opportunity to relax. The structural changes during this process will be characterized with the help of a transition function $C(t)$, which is defined as

$$C(t) = \frac{\langle \mathcal{A}(t) \rangle - \langle \mathcal{A}^{v=0} \rangle}{\langle \mathcal{A}(t_1) \rangle - \langle \mathcal{A}^{v=0} \rangle} \tag{8}$$

where $\mathcal{A}$ denotes the observable of interest, that is, end-to-end distance and average inclination. t_1 is defined as the time at which sliding is reinitiated, and $\langle \mathcal{A}^{v=0} \rangle$ denotes the expectation value of the observable $\mathcal{A}$ at zero-stress equilibrium. The transition functions of the squared end-to-end vector and the inclination angle are shown in Figure 9 as a function of time for a relaxation time $t_{rel} = 50$. The time axis is expressed in units of τ_{rheo}, which is defined as the time at which the free endgroup reacts to the reinitialization of motion, that is, where $\partial C(t)/\partial t$ becomes positive.

After sliding is reinitiated, polymers stretch and incline in a characteristic fashion. For all velocities and relaxation times employed in this study, no swelling is observed during this itinerant go phase. The only observable that shows quite universal behavior is the number of interactions N_{int}, which decays exponentially with time toward the steady-sliding value, once sliding is reinitiated. This is shown on the left-hand-side of Figure 10. The corresponding relaxation time increases strongly with decreasing velocity v, which is again indicative of the far-from-equilibrium nature of the system.

It is interesting to note that the shear force does not show a significant overshoot (stiction peak) (see the right-hand-side of Figure 10), which is again in contrast to the stop-and-return protocol. Only for the two large velocities $v = 0.15$ and $v = 0.25$, a small hump in the shear force is observed, which is indicative of the mechanical contact's structural relaxation. There is no characteristic length or other scaling concept that would allow us to superimpose data as well as we could for the stop-and-return protocol in Figure 8.

Summarizing, we confirm our previous result that the shear forces decay more rapidly than the polymer structure; in particular, σ_{br} decays more rapidly than the inclination of the end-to-end vector.[15] However, indirect

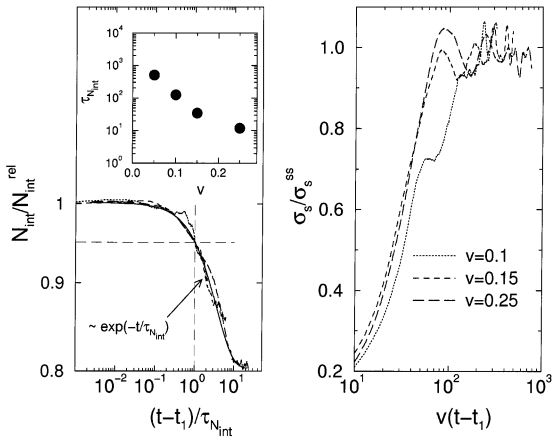

Figure 10. Left: Number of interactions as a function of time. The time axis is rescaled so that all data collapse on the same point at unity. Inset: Characteristic time as a function of velocity. Right: Shear stress as a function of driven distance.

information about the degree of structural relaxation can be obtained by comparing the stop-and-go and the stop-and-return protocol. If the structural relaxation is not complete yet, larger shear stress maxima will be found if the sliding direction is inverted than if the sliding is continued parallel to the original direction.

IV. Conclusions

In this paper, we presented the study of a generic model for the relative, sliding motion of two surfaces bearing end-anchored polymers in good solvent conditions. Our focus was on contrasting stationary and nonstationary sliding modes. The two nonstationary sliding modes follow two different protocols: (i) stop and return and (ii) stop and go. In either case, the system can relax for some time before sliding is reimposed.

The strong correlation between shear forces and mutual brush overlap observed previously[1] is found to persist, even though in the new study, the thermostat does not act in the sliding direction. The overlap controls friction not only during stationary sliding but also in nonstationary conditions. If the sliding direction is inverted, the brushes swell, which leads to an enhanced brush overlap during the itinerant return phase. This swelling is reflected in a pronounced maximum of the shear stress σ_{br}. The swelling is also consistent with the increase of the normal forces reported during oscillatory shear flow.[5]

Shear stresses are maximal in the stop-and-return protocol when the average inclination of the polymers passes through 90°. The characteristic distance $\mathcal{A}_c$ that the upper wall has to be moved relative to the lower wall for the shear stress maxima to occur is found to be *twice* the lateral extension l_c of the polymers in steady-state, constant-velocity conditions. Hence, experiments employing oscillatory shear might allow one to determine the polymer's inclination under constant-velocity conditions rather precisely. In a limited range of velocities, l_c is found to be proportional to $v^{0.3}$, where v is the relative sliding velocity. Although the exponent 0.3 is not universal, that is, it depends on the ratio of grafting density and critical grafting density, it would be interesting to check experimentally for a power-law behavior. This could be done for example using oscillatory shear, where $\mathcal{A}$ would have to be associated with the driving amplitude and the velocity v would roughly equal $\mathcal{A}\omega$ with ω being the driving frequency. Note that the predicted shear stress maxima (or maxima in effective viscosity) for $\mathcal{A} \approx 2l_c$ are the consequence of the strong nonequilibrium state of the

brushes. Since the system is far out of equilibrium, these maxima cannot be related to an intrinsic relaxation time of the embedded system as is frequently done in the analysis of rheological data.[11] At the same time, it is not necessary to assume stick−slip motion for the occurrence of enhanced dissipation, which otherwise can lead to enhanced dissipation.[12]

In a previous study,[15] we found that shear stress relaxation does not imply structural relaxation of the polymers. In the terminology of this paper, ref 15 corresponded to a "stop-and-wait" protocol, for which we found that the inclination angle of the end-to-end vector decays much more slowly than the shear stress. However, if one compares the shear stress maxima that one observes with the (i) stop−wait−return protocol with those from the (ii) stop−wait−go protocol, more information can be revealed. The shear stress maximum in σ_{br} is more pronounced for (i) than for (ii) if there is hysteresis in the orientation of the polymers. Relaxation cannot be complete until the difference in the σ_{br} maxima has disappeared for protocols i and ii. Figuratively speaking, combing out, away from the part in the hair, requires less effort than combing the hair in the opposite direction. However, if hair is left alone to nature (wind, poor hygiene, etc.) for a long period of time, combing in either direction eventually becomes equally difficult.

As in one of our previous studies,[15] we want to emphasize that possible new effects may emerge in experiments due to energy-driven instabilities such as cis−trans conformation changes in the polymers. In fact, Cai et al. observe two maxima in the shear loss $G''(\omega)$ (see Figure 2 in ref 10). Only one of these can be related to the phenomenon central to this study, while the other one might be related to sliding-induced cis−trans conformation changes. This and other thermally activated configuration changes are absent in our simple bead−spring model that emphasizes the entropic excluded-volume interactions between polymers in good solvents. Local cis−trans conformation transitions will presumably induce stronger aging effects for both protocols, stop-and-return and stop-and-go. Nevertheless, we do not expect strong deviation from our main conclusions.

Another important difference between simulations and experiments for the stop-and-go protocol concerns the use of periodic boundary conditions in the simulations. Thus, the predictions relating to the stop-and-go protocol relate better to journal-bearing or "wheel-on-the-road" geometries than to the geometry employed in surface force apparatus experiments.

Acknowledgment. Partial support is acknowledged from the Bundesministerium für Bildung und Forschung (BMBF), Grants No. 03N6016 and 03N6500, and via Project DIP352-101.

LA030008X